Contrib Mineral Petrol (2005) 150: 441–455
DOI 10.1007/s00410-005-0022-y

ORIGINAL PAPER

Gültekin Topuz · Rainer Altherr
Winfried H. Schwarz · Wolfgang Siebel
Muharrem Satır · Abdurrahman Dokuz

Post-collisional plutonism with adakite-like signatures: the Eocene Saraycık granodiorite (Eastern Pontides, Turkey)

Received: 7 February 2005 / Accepted: 23 June 2005 / Published online: 7 October 2005

Abstract The post-collisional Saraycık granodiorite intruded into a late Paleocene to early Eocene nappe pile that formed during collision of the Pontides in the North and the Anatolide-Tauride platform in the South, leading to the formation of the İzmir-Ankara-Erzincan suture. A relatively shallow pluton intrusion depth (~5 to 8 km) was estimated from Al-in-hornblende geobarometry and contact metamorphic assemblages. The emplacement age is tightly constrained to ~52 Ma by two Ar–Ar plateau and total fusion ages on biotite. The main mass of the pluton consists of metaluminous to peraluminous biotite granodiorite and hornblende-biotite granodiorite. In addition, up to 10-m thick dacitic and <25-cm thick aplitic dikes occur. Granodiorites and dacites show many close compositional similarities to high-silica adakites from supra-subduction zone settings, but tend to be slightly more felsic and to have a higher aluminium saturation index. Chondrite-normalized (cn) rare earth element patterns are characterized by high ratios of $(La/Yb)_{cn}$, concave-upward shapes of the HREE and a lack of significant Eu anomalies. In conjunction with relatively high abundances of Ba and Sr as well as low abundances of Y, HREE and Sc, these patterns suggest a feldspar-poor, garnet ± amphibole-rich fractionating mineral assemblage (residue). All samples have very similar Nd–Sr isotopic characteristics, regardless of rock type. Initial ε_{Nd} values range from −0.3 to −1.2 and initial $^{87}Sr/^{86}Sr$ ratios from 0.70491 to 0.70529. It is suggested that the magmas formed by partial melting of mafic lower crust at elevated pressures (~1 to 2 GPa).

Communicated by J. Hoefs

G. Topuz (✉) · A. Dokuz
Department of Geology, Black Sea Technical University (KTÜ), TR-61080 Trabzon, Turkey

R. Altherr · W. H. Schwarz
Institute of Mineralogy, University of Heidelberg, Im Neuenheimer Feld 236, 69120 Heidelberg, Germany
E-mail: raltherr@min.uni-heidelberg.de
Tel.: +49-6221-548207
Fax: +49-6221-544805

W. Siebel · M. Satır
Institute of Geosciences (Geochemistry), University of Tübingen, Wilhelmstr. 56, 72074 Tübingen, Germany

Present address: G. Topuz
Eurasian Institute of Earth Sciences, Technical University of Istanbul (İTÜ), Ayazaga, 80626 Istanbul, Turkey
E-mail: topuzg@itu.edu.tr
Tel.: +90-212-2856112
Fax: +90-212-2856210

Introduction

Silicic Na-rich igneous rocks characterized by low abundances of HREE, Y and Sc, high abundances of Ba and Sr, and resulting high Sr/Y and La/Yb ratios include members of the Archaean TTG suite, Cenozoic high-silica adakites and Phanerozoic Na-rich granitoids. Compositional similarities and differences between these rock types have been discussed extensively by Smithies (2000), Condie (2005), and Martin et al. (2005). The genesis of the magmas, however, is still a matter of debate (e.g. Smithies 2000; Yumul et al. 2000; Garrison and Davidson 2003; Prouteau and Scaillet 2003; Condie 2005; Martin et al. 2005). While it is generally accepted that the presence of significant amounts of garnet ± amphibole are required at some stage in the petrogenesis of these magmas, either as a residual or an early crystallizing phase assemblage, a variety of petrogenetic models have been proposed, including (1) melting of the basaltic portion of the subducted oceanic lithosphere (e.g. Defant and Drummond 1990, 1993; Drummond and Defant 1990; Kay et al. 1993) and subsequent variable interaction of slab-derived melts with the peridotitic mantle wedge (e.g. Stern and Kilian 1996; Rapp et al. 1999, 2005; Smithies 2000; Prouteau et al. 2001); (2) high-pressure fractionation of garnet and amphibole from hydrous basaltic magma (Prouteau

and Scaillet 2003); (3) partial melting of hot mafic lower arc crust, triggered by underplating of basaltic magmas and/or release of fluids from underthrust continental rocks (e.g. Smith and Leeman 1987; Atherton and Petford 1993; Wareham et al. 1997; Yumul et al. 2000; Chung et al. 2003; Rapp et al. 2003; Garrison and Davidson 2003; Stevenson et al. 2005; Wang et al. 2005); (4) derivation of magmas from ancient mafic lower continental crust (eclogite) that foundered into the convecting mantle and subsequently melted and interacted with peridotite (Xu et al. 2002; Gao et al. 2004).

This study deals with the genesis of a post-collisional high-Sr/Y granodiorite/dacite pluton from the Eastern Pontides (NE Turkey) that was emplaced ~52 Ma ago into a late Paleocene nappe pile, generated during the collision of the Pontides and the Tauride-Anatolide platform that followed the northward subduction of the northern branch of Neotethys. Based on field relationships, rock textures, mineral compositions, whole-rock chemical analyses and Sr–Nd isotopic data, it is suggested that the adakite-like magmas formed by partial melting in the mafic lower crust at a depth of ≥35 km.

Geological setting

The Eastern Pontides in NE Turkey are classically divided into a northern and a southern zone that differ from each other in terms of rock associations. In the northern zone, late Cretaceous to Eocene volcanic rocks with Kuroko-type ore deposits and coeval granitoids predominate. The southern zone is a multi-phase tectonic collage comprising mainly plutonic, metamorphic and sedimentary rocks of pre-late Cretaceous age (Akın 1979; Gedikoğlu et al. 1979; Okay and Şahintürk 1997; Okay et al. 1997; Topuz et al. 2004a, b). While Permian to pre-Liassic events are generally ascribed to the consumption of Paleotethys, ophiolite obduction during the Cenomanian as well as Cretaceous to Eocene magmatism and a late Paleocene to early Eocene phase of northward thrusting are generally attributed to northward subduction of the northern branch of Neotethys and subsequent collision between the Pontides in the North and the Tauride-Anatolide platform in the South (e.g. Akın 1979; Gedikoğlu et al. 1979; Şengör and Yılmaz 1981; Akıncı 1984; Robinson et al. 1995; Yılmaz and Boztuğ 1996; Okay et al. 1996, 1997, 2002; Arslan et al. 1997; Okay and Monié 1997; Okay and Şahintürk 1997; Yılmaz et al. 1997; Şen et al. 1998; Okay 2000; Topuz et al. 2004a; Boztuğ et al. 2004). Both the onset of subduction and the timing of collision between the Pontides and the Anatolide-Tauride platform have been a matter of debate (e.g. Tokel 1977; Akın 1979; Robinson et al. 1995; Okay and Şahintürk 1997; Boztuğ et al. 2004). Ar–Ar laser probe dating on phengite grains from high-*P* low-*T* metamorphic jadeite schists in the western Pontides along the İzmir-Ankara-Erzincan Suture yielded ages between 88 and 70 Ma (Okay and Kelley 1994), suggesting that the collision should be late Cretaceous or younger. Taking into account that nappe tectonics in the eastern Pontides was dated as late Paleocene to early Eocene, based on field relationships and ages of cross-cutting granitoids, and the fact that Eocene and younger formations are unfolded and transgressively overlie the thrust planes, a late Paleocene to early Eocene age for the collision seems probable (Okay and Şahintürk 1997; Okay et al. 1997).

The Saraycık intrusion is located in the northeastern part of the Pulur complex belonging to the southern Pontides (Okay et al. 1997; Topuz et al. 2004a, b) and crops out over an area of ~11 km^2 (Figs. 1, 2). The granodiorite pierced the late Paleocene to early Eocene tectonic contact between the Hamurkesen and Asutka thrust sheets (Fig. 1) and caused a ~0.8 km wide contact aureole visible in (1) Permocarboniferous clastic sediments, (2) Permian low-grade phyllites and greenschists of the Doğankavak unit, and (3) Carboniferous high-grade gneisses, migmatites and amphibolites of the Cenci unit (Fig. 2). The main mass of the pluton consists of fine- to medium-grained granodiorite that occurs in two petrographic varieties; hornblende-free biotite granodiorite seems to form the main mass of the pluton, while hornblende-biotite granodiorite is subordinate and was found in the southern part of the pluton (Fig. 2). The granodiorites locally contain up to 10 m thick dacitic and < 25 cm thick aplitic dikes as well as later hydrothermal quartz veins. Outcrop conditions did not allow to establish age relationships between the different granodiorite varieties and between the two compositionally different types of dikes. Some of the aplitic dikes show coarse-grained quartz-rich inner zones suggestive of the infiltration of late-stage volatile-rich melts or silicate-rich aqueous fluids. In the eastern part of the pluton, a few microgranular mafic enclaves with ovoid shapes (up to 10 cm in diameter) occur. Their contacts with the host granodiorite vary from sharp to gradational. No country rock-derived xenoliths were found. Although the main mass of the pluton is undeformed, thin shear zones are locally developed.

Analytical techniques

Aliquots for bulk-rock chemical analyses were obtained by quarter reduction of split from samples weighting 1–3 kg. Major elements and the trace elements Rb, Ba, Sr, Y, Zr, Pb, Ga, Zn, Ni, V, Cr, Nb and Th were determined by XRF (modernized SRS 300 wavelength-dispersive spectrometer; Bruker AXS) at Heidelberg. Lithium borate fusion disks and pressed powder tablets were used for major and trace elements, respectively. Calibration was performed with international reference samples. The trace elements Cs, Sc, Ta, U, HF and the rare earth elements (REEs) were determined at the commercial Acme Analytical Laboratories Ltd at Vancouver, Canada. 0.2 g sample powder and 1.5 g $LiBO_2$ flux were mixed in a graphite crucible and subsequently

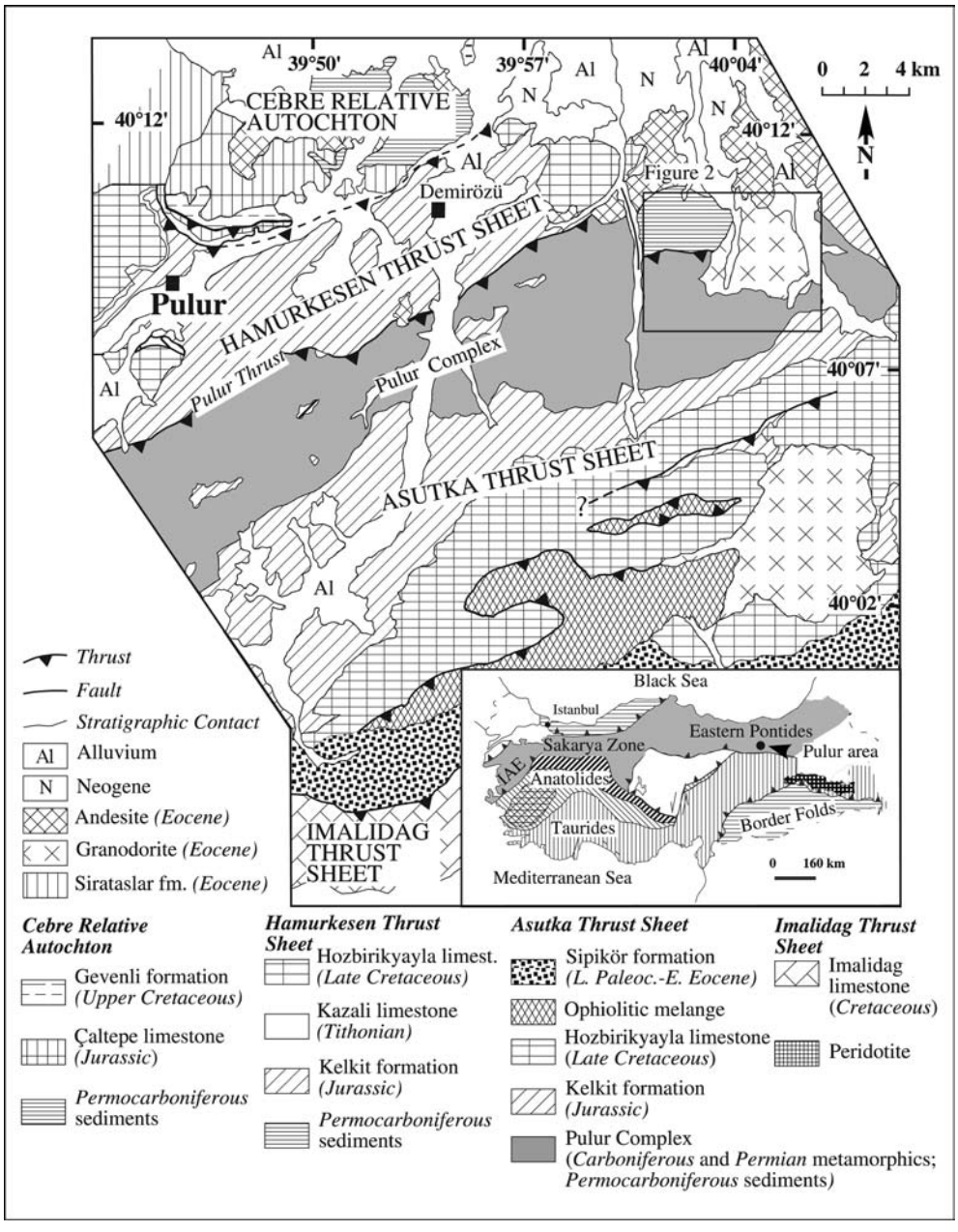

Fig. 1 Generalized map of the Pulur area (modified after Okay et al. 1997). Inset shows main tectonic units of Turkey (modified after Okay 1986)

heated to 1,050°C for 15 min. The molten sample was then dissolved in 5% HNO_3 (ACS grade nitric acid diluted in demineralized water). Calibration standards and reagent blanks were added to the sample sequence. Sample solutions were aspirated into an ICP mass spectrometer (Perkin-Elmer Elan 6000).

Rb–Sr and Sm–Nd isotope analyses were performed at the Institute of Geosciences at Tübingen. Rock powders were dissolved in 52% HF for 4 days at 140°C on a hot plate. Digested samples were dried and redissolved in 6 N HCl, dried again and redissolved in 2.5 N HCl. Sr and light REEs were isolated on quartz columns by conventional ion exchange chromatography with a 5 ml resin bed of Bio Rad AG 50W-X12, 200–400 mesh. Nd was separated from other REEs on quartz columns using 1.7 ml Teflon powder coated with HDEHP, di(2-ethylhexyl)orthophosphoric acid, as cation exchange medium. All isotopic measurements were made by thermal ionization mass spectrometry using a Finnigan MAT 262 mass spectrometer. Sr was loaded with a Ta–HF activator on pre-conditioned W filaments and was measured in single-filament mode. Nd was loaded as phosphate on pre-conditioned Re filaments and measurements were performed in a Re double filament configuration. The $^{87}Sr/^{86}Sr$ isotope ratios were normalized to $^{86}Sr/^{88}Sr = 0.1194$ and the $^{143}Nd/^{144}Nd$ isotope ratios to $^{146}Nd/^{144}Nd = 0.7219$. The La Jolla Nd-Standard yielded a value of 0.511836 ± 0.000007 (reference value 0.511850) and the NBS 987 Sr standard yielded $^{87}Sr/^{86}Sr$ ratios of 0.710248 ± 0.000008 (reference value 0.710240). Total procedural blanks (chemistry and loading) were 134 pg for Nd and 333 pg for Sr.

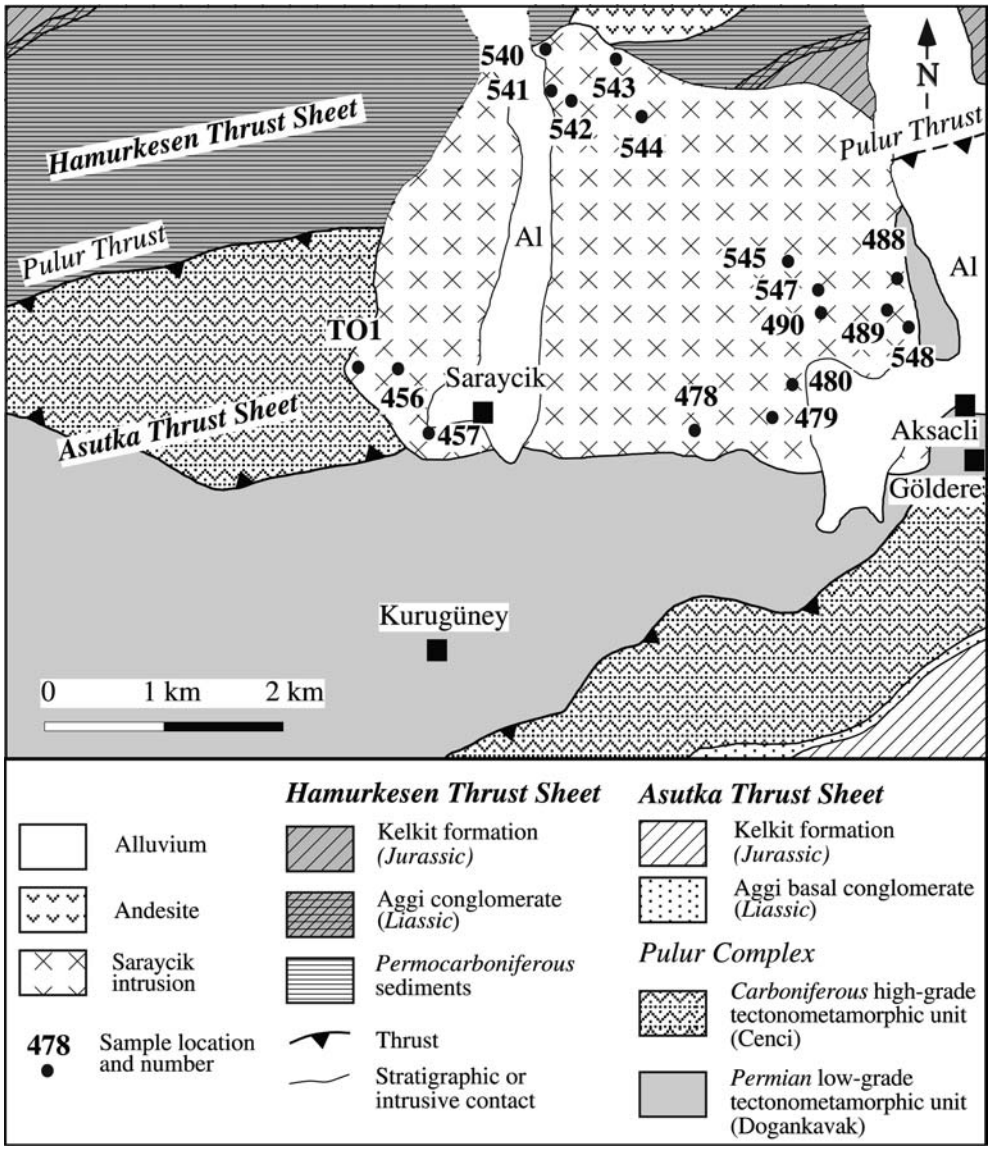

Fig. 2 Geological map of the Saraycık intrusion with sample locations

Mineral analyses were carried out at the Institute of Mineralogy at Heidelberg with a CAMECA SX51 electron microprobe equipped with five wavelength-dispersive spectrometers and an additional Si–Li detector (Oxford Instruments). Standard operating conditions were 15 kV accelerating voltage, 20 nA beam current and a beam diameter of ~1 μm. Counting times were usually 10 s except for Mg, Ca and Al (20 s) and Ti (30 s) in oxides. Feldspars were analysed with a defocused beam (10 μm) in order to minimize loss of alkalis. Natural and synthetic oxide and silicate standards were used for calibration. The PAP algorithm (Pouchou and Pichoir 1984, 1985) was applied to raw data. Detection limits are generally on the order of 0.1 wt%.

$^{40}Ar/^{39}Ar$ dating was performed at the Institute of Mineralogy at Heidelberg. Biotite separates were obtained by conventional techniques including cracking, sieving, magnetic and heavy liquid separation, handpicking and ultrasonic cleaning. Irradiation of the Al-wrapped samples within an evacuated and Cd-shielded quartz tube with $\sim 1.5 \times 10^{18}$ fast neutrons/cm^2 was performed in the FRG-1 reactor of the Nuclear Research Center Geesthacht, Germany. Age and irradiation gradient monitoring was achieved by an in-house muscovite standard (muscovite 'BMus', 326.2 ± 1.1 Ma, 1σ). Ar was extracted in a resistance-heated Ta furnace in a double-vacuum system up to 1,600°C. First, H_2O and CO_2 from the extracted gas were frozen by using an acetone-CO_2 mixture. For further cleaning, Zr–Al getters were used. Ar isotope compositions were measured in a MAT GD-150 gas mass spectrometer (0.38 T permanent magnet, 180°, 5 cm radius of curvature). Constants used for age calculations are those recommended by Steiger and Jäger (1977). $^{40}Ar/^{39}Ar$ age uncertainties comprise the errors of the $^{40}Ar/^{39}Ar$ ratios of irradiation monitors and the age errors of the monitor. Measured $^{40}Ar/^{39}Ar$ data were corrected for irradiation interferences. Analytical procedures applied during the mea-

surements correspond to those of Hradetzky and Lippolt (1998) and Schubert et al. (2001). All error assignments of isotope ratios and ages given within this paper are $\pm 1\sigma$.

Results

Petrography and mineral compositions

Granodiorites have fine- to medium-grained (0.5–5.0 mm) textures with larger hypidiomorphic plagioclase grains in a finer-grained matrix of plagioclase, biotite, quartz and perthitic orthoclase (Fig. 3a, b). Only in some samples (455 and 489) hornblende is present as an additional phase. Most plagioclase grains show normal oscillatory zoning with An_{44} to An_{07} (Fig. 3a) but some grains show a complex interior with patchy (An-rich and An-poor) cores overgrown by An-poor rims (Fig. 3b). The crystallization of perthitic orthoclase (bulk composition $Or_{96\text{-}83}Ab_{04\text{-}17}An_{01\text{-}00}$) started rather late, after the onset of biotite and quartz crystallization (Fig. 3a, b). Biotite is Al-poor and has variable TiO_2 contents (2.3–4.1 wt%) and X_{Mg} [$= Mg/(Mg + Fe_{tot})$] of 0.54 to 0.63 (Table 1). Green magnesiohornblende is characterized by $Na/K = 3.1$–5.6 and $X_{Mg} = 0.66$–0.73 (Table 1). Primary accessory phases are magnetite, Fe–Ti oxides, titanite, allanite, apatite and zircon. Titanite is more abundant in hornblende granodiorite and often contains inclusions of resorbed exsolved Fe–Ti oxides and quartz (Fig. 3c). Fe–Ti oxides were not observed outside titanite. Apatite forms rod-like to euhedral prismatic grains that occur as inclusions in biotite, hornblende and plagioclase. Zircon forms long euhedral crystals; rounded or irregularly shaped zircon grains were not observed. Some granodiorite samples show hydrothermal alteration with secondary carbonate, hematite, sericite, kaolinite and chlorite.

Microgranular mafic enclaves have a monzodioritic composition and consist of plagioclase, biotite and subordinate orthoclase (Fig. 3d, e), accompanied by accessory apatite, magnetite and zircon. The composition of biotite is similar to those of the granodiorite (Table 1). Plagioclase shows An-rich ($An_{53\text{-}38}$) domains replaced by less An-rich plagioclase ($An_{23\text{-}17}$) (Fig. 3d).

Dacitic dikes show a porphyritic texture with phenocrysts of plagioclase, biotite and hornblende (0.3–2.0 mm) in a fine-grained matrix of quartz, plagioclase, hornblende, biotite, orthoclase, magnetite and apatite (Fig. 3f–h). Biotite phenocrysts often contain relatively large inclusions of inversely zoned plagioclase ($An_{31\text{-}37}$ in the core, $An_{38\text{-}40}$ at the rim) and have corroded margins with newly formed ilmenite (Fig. 3f). Larger grains show a slight zoning with a core-to-rim increase of X_{Mg} from 0.54 to 0.56, while groundmass biotite tends to be even more magnesian (Table 1). Plagioclase phenocrysts are of two distinct types. The first one is characterized by sieved cores ($An_{61\text{-}23}$) overgrown by thin clear rims ($An_{49\text{-}37}$) (Fig. 3g), while the second type shows normal oscillatory zoning ($An_{46\text{-}33}$) and is overgrown by thin An-rich ($An_{47\text{-}50}$) rims (Fig. 3h). Matrix plagioclase has $An_{27\text{-}25}$. Hornblende forms needles and is largely altered to chlorite and calcite. Hornblende relicts are compositionally similar to hornblende from the granodiorite (Table 1).

Aplitic dikes consist of quartz, plagioclase, orthoclase and minor biotite, apatite, zircon and titanite. Some of these dikes are composite with quartz-rich inner zones.

Depth of intrusion

The Saraycık granodiorite contains the critical mineral assemblage hornblende + biotite + plagioclase + K-feldspar + quartz + titanite + Fe–Ti oxide + apatite that together with melt is required for the application of Al-in-hornblende barometer (Anderson and Smith 1995 and references therein). Since K-feldspar was a late crystallizing phase, we used the compositions of hornblende rims in contact with interstitial quartz and/or orthoclase (Table 1) for estimating the pressure at which late-stage (near-solidus) crystallization of the granodioritic magma occurred. An average pressure of 0.21 ± 0.05 GPa (1σ) at an assumed temperature of 700°C (wet solidus of granodiorite; e.g. Johannes and Holtz 1996) was obtained. This value is in line with the presence of the assemblage andalusite + corundum + K-feldspar in contact metamorphic rocks, implying a maximum pressure of ~0.25 GPa (see, for example, grids given in Pattison et al. 2002). In conclusion, an emplacement depth of ~5–8 km is inferred.

Ar–Ar dating

Biotite separates from granodiorite samples TO1 and 479 yielded $^{40}Ar/^{39}Ar$ total fusion ages of 52.8 ± 0.4 (1σ) and 51.9 ± 0.5 Ma, respectively (Table 2). Stepwise heating gave rather flat age spectra, corresponding to 'plateau ages' of 52.1 ± 0.7 and 51.8 ± 0.4 Ma (Fig. 4). All these ages are identical within error. Thermal relaxation of the relatively small granodiorite pluton and its contact aureole should have occurred within a time span of less than 1 Ma, as suggested by simple calculations using models and data from Jaeger (1957). Closure temperature of biotite for Ar diffusion is around 345–310°C (Harrison et al. 1985; Grove and Harrison 1996; Villa 1998). Therefore, the biotite cooling ages of ~52 Ma (Ypresian) are regarded as a good approximation for the intrusion age.

Whole-rock chemistry

Major and trace element compositions of representative samples from the granodiorite and the dacitic and aplitic dikes are given in Table 3. Samples of fresh biotite granodiorite are metaluminous to peraluminous with ASI [$=$ molar $Al_2O_3/(CaO + K_2O + Na_2O)$] ranging

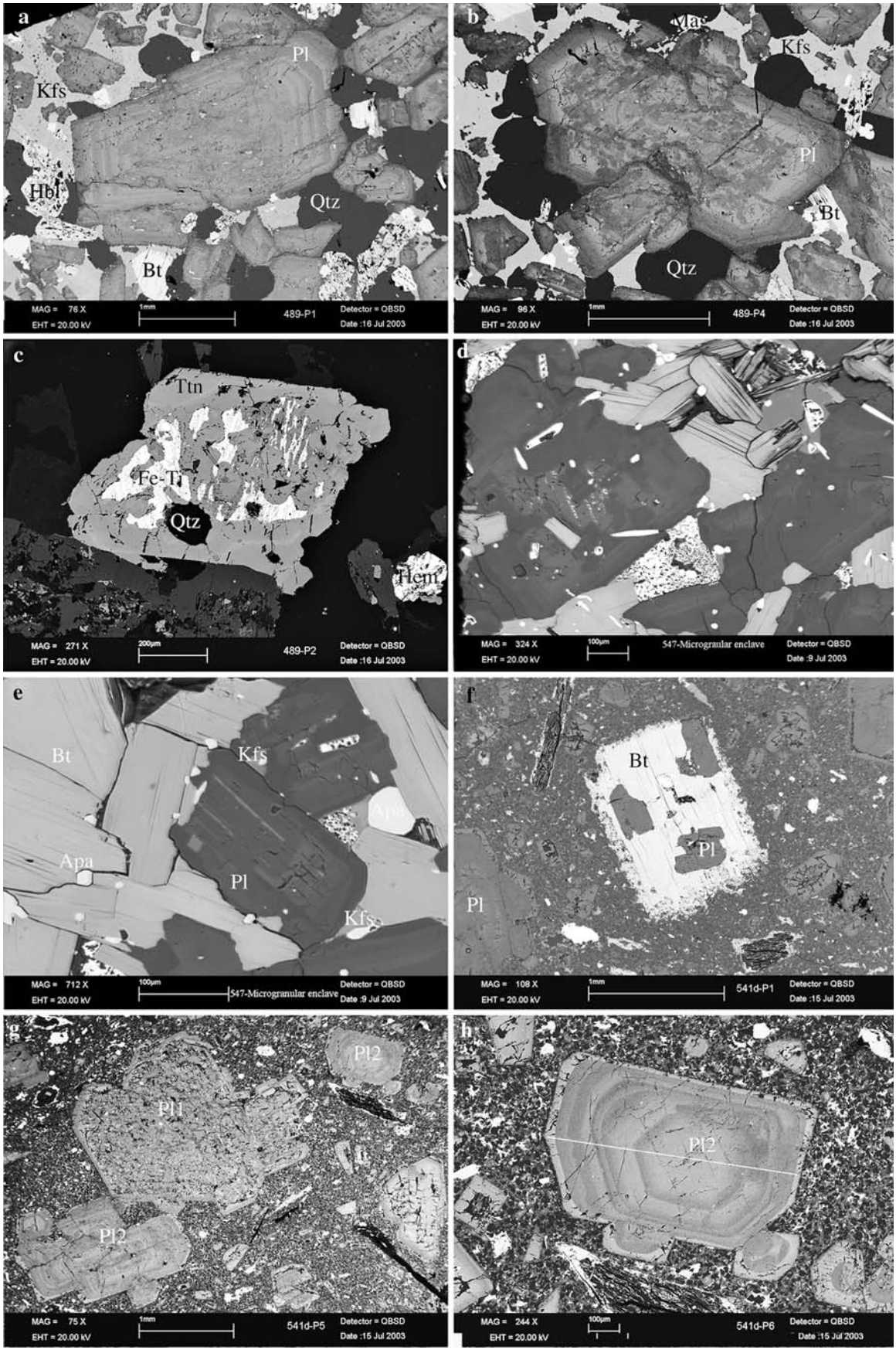
a
Pl
Kfs
Hbl
Qtz
Bt
MAG = 76 X
EHT = 20.00 kV
1mm
489-P1
Detector = QBSD
Date :16 Jul 2003
b
Kfs
Pl
Bt
Qtz
MAG = 96 X
EHT = 20.00 kV
1mm
489-P4
Detector = QBSD
Date :16 Jul 2003
c
Ttn
Fe-Ti
Qtz
Hem
MAG = 271 X
EHT = 20.00 kV
200µm
489-P2
Detector = QBSD
Date :16 Jul 2003
d
MAG = 324 X
EHT = 20.00 kV
100µm
547-Microgranular enclave
Detector = QBSD
Date :9 Jul 2003
e
Bt
Kfs
Apa
Pl
Kfs
MAG = 712 X
EHT = 20.00 kV
100µm
547-Microgranular enclave
Detector = QBSD
Date :9 Jul 2003
f
Bt
Pl
Pl
MAG = 108 X
EHT = 20.00 kV
1mm
541d-P1
Detector = QBSD
Date :15 Jul 2003
g
Pl2
Pl1
Pl2
MAG = 75 X
EHT = 20.00 kV
1mm
541d-P5
Detector = QBSD
Date :15 Jul 2003
h
Pl2
MAG = 244 X
EHT = 20.00 kV
100µm
541d-P6
Detector = QBSD
Date :15 Jul 2003

◀

Fig. 3 Back-scattered electron images showing textural features of the Saraycık granodiorite and associated rocks. **a** Plagioclase (*Pl*) with normal oscillatory zoning surrounded by finer-grained matrix of hornblende (*Hbl*), biotite (*Bt*), quartz (*Qtz*), K-feldspar (*Kfs*) and plagioclase. Granodiorite 489. **b** Plagioclase with patchy interior (An-rich and An-poor) cores overgrown by An-poor rims. Granodiorite 489. **c** Titanite with inclusions of exsolved Fe–Ti oxides and quartz. Granodiorite 489. **d** Plagioclase grain with relictic An-rich (An_{53-38}) domains replaced by less An-rich outer zones (An_{23-17}). Microgranular mafic enclave 547. **e** Plagioclase and biotite (*Bt*) with interstitial apatite (*Apa*) and K-feldspar (*Kfs*). Microgranular mafic enclave 547. **f** Phenocrysts of marginally corroded biotite (*Bt*) and plagioclase (*Pl*) in a fine-grained matrix composed of quartz, plagioclase, K-feldspar, biotite and magnetite. Dacitic dike 541d. **g** Two types of plagioclase phenocrysts in dacitic dike. Pl1 has sieved texture and Pl2 shows normal oscillatory zoning, surrounded by a thin An-rich rim. Sample 541d. **h** Close-up picture of Pl2 plagioclase from upper right corner in **g**

from 0.98 to 1.13 (Table 3). The hornblende-biotite granodiorite and the microgranular enclave (sample 547) are metaluminous (ASI = 0.99–0.90), while the dacitic and aplitic dikes are peraluminous. Sample 480 shows an exceptionally high ASI value of 1.32, caused by significant amounts of secondary kaolinite and sericite due to hydrothermal alteration. Minor amounts of sericite, chlorite and carbonate are also present in samples 541A and 542.

The granodiorite and the dacitic dikes span a narrow compositional range with SiO_2 between ~65 and 70 wt%, while the aplitic dikes have SiO_2 between 74.7 and 77.1 wt% (Table 3, Fig. 5). Most granodiorite and all dacite samples belong to the medium-K series (Fig. 5a). Two samples of biotite granodiorite from the southwestern part of the pluton (TO1 and 456; Fig. 2), however, plot into the field of the high-K series. In addition, these two samples are characterized by lower MgO contents and higher abundances of Ba, Y, Zr, Nb, Ta, Th and REE, as compared to the other granodiorite samples (Table 3, Fig. 5). On the basis of these chemical differences, two groups of biotite granodiorite have been distinguished (BG1 and BG2; Table 3). The samples of hornblende-biotite granodiorite (HBG) have higher contents of MgO than BG1 and BG2 samples (Fig. 5d), while the abundances of Y are between those of BG1 and BG2 (Fig. 5o).

Compared to other occurrences of post-collisional granodiorite, such as in the Variscan belt of Central Europe (Altherr et al. 2000) or in the Central Aegean area (Altherr and Siebel 2002), the abundances of Yb, Y and Sc in the Saraycık rocks are relatively low and those of Sr and Ba are high (Table 3). Chondrite-normalized (cn) REE patterns of granodiorite and dike rock samples have HREE concave-upward shapes and are characterized by the general absence of a significant Eu anomaly

Table 1 Selected electron microprobe analyses of hornblende and biotite from the Saraycık pluton

Mineral	Hbl	Hbl	Hbl	Hbl	Hbl	Hbl	Hbl	Hbl	Hbl	Bt	Bt	Bt	Bt	Bt	Bt	Bt	Bt	Bt
Sample	455	455	455	455	489	489	489	489	541B	TO1	541A	544A	547	547	455	489	541B	541B
Rock type	HBG	HBG	HBG	HBG	HBG	HBG	HBG	HBG	D	BG1	BG2	BG2	ME	ME	HBG	HBG	D	D
Area	Rim	Core	Core	Rim	Core	Rim	Rim	Core	Small	Core	Core	Core	Core	Core	Core	Core	Core	Rim
SiO_2	51.08	51.18	50.79	51.10	49.78	51.92	49.58	48.70	47.79	37.29	36.92	36.87	36.76	37.19	37.85	36.85	36.94	39.46
TiO_2	0.59	0.66	0.63	0.63	0.80	0.59	0.67	0.92	0.96	3.18	3.67	3.75	3.99	3.24	4.04	3.76	3.83	2.63
Al_2O_3	4.03	4.11	4.22	4.05	5.95	4.13	4.86	5.87	6.79	13.65	13.91	13.52	13.20	13.75	13.36	13.01	13.53	14.41
Cr_2O_3	0.01	0.02	0.06	0.00	0.00	0.00	0.00	0.00	0.01	n.a.	n.a.	n.a.	n.a.	n.a.	n.a.	n.a.	n.a.	n.a.
FeO_{tot}	11.59	11.98	11.97	12.17	13.20	12.05	12.42	12.59	14.75	16.37	16.90	18.18	16.91	16.93	16.00	15.97	17.76	16.41
MnO	0.78	0.68	0.64	0.74	0.68	0.82	0.62	0.43	0.57	1.12	0.43	0.38	0.43	0.49	0.49	0.31	0.27	0.25
MgO	15.40	15.48	15.45	15.58	14.25	15.61	15.20	14.78	13.94	13.46	13.91	13.55	13.58	13.99	13.32	13.70	13.64	12.87
CaO	11.62	11.75	11.89	11.68	11.52	11.81	11.62	11.56	11.46	0.00	0.08	0.00	0.00	0.00	0.04	0.02	0.00	0.04
Na_2O	0.80	0.85	0.60	0.73	1.29	0.89	1.01	1.35	1.04	0.06	0.13	0.11	0.10	0.09	0.14	0.11	0.21	0.06
K_2O	0.35	0.32	0.32	0.35	0.35	0.41	0.42	0.49	0.38	9.14	8.96	9.16	9.27	9.32	9.16	9.29	8.98	8.41
Total	96.25	97.04	96.58	97.02	97.83	98.23	96.41	96.69	97.69	94.27	94.90	95.52	94.24	94.98	94.40	93.02	95.14	94.61
Cations on the basis of 23 oxygens (hornblende) and 11 oxygens (biotite)																		
Si	7.449	7.415	7.386	7.400	7.209	7.433	7.257	7.135	6.947	2.847	2.799	2.798	2.816	2.821	2.870	2.845	2.804	2.952
$Al^{[IV]}$	0.551	0.585	0.614	0.600	0.791	0.567	0.743	0.865	1.053	1.153	1.201	1.202	1.184	1.179	1.130	1.155	1.196	1.048
$Al^{[VI]}$	0.141	0.116	0.109	0.091	0.225	0.130	0.096	0.149	0.110	0.075	0.042	0.007	0.008	0.050	0.064	0.029	0.015	0.223
Ti	0.065	0.072	0.069	0.069	0.087	0.064	0.074	0.101	0.105	0.183	0.209	0.214	0.230	0.185	0.230	0.219	0.219	0.148
Cr	0.001	0.002	0.007	0.000	0.000	0.000	0.000	0.000	0.001	–	–	–	–	–	–	–	–	–
Fe^{3+}	0.227	0.240	0.289	0.304	0.248	0.233	0.324	0.260	0.597	0.000	0.000	0.000	0.000	0.000	0.000	0.000	0.000	0.000
Fe^{2+}	1.186	1.211	1.167	1.169	1.351	1.209	1.196	1.282	1.196	1.045	1.071	1.153	1.083	1.074	1.015	1.031	1.128	1.027
Mn	0.096	0.083	0.079	0.091	0.083	0.099	0.077	0.053	0.070	0.072	0.028	0.024	0.028	0.032	0.031	0.020	0.017	0.016
Mg	3.348	3.343	3.350	3.363	3.077	3.332	3.317	3.228	3.021	1.532	1.572	1.532	1.550	1.582	1.506	1.577	1.544	1.436
Ca	1.815	1.824	1.852	1.812	1.787	1.811	1.822	1.815	1.785	0.000	0.006	0.000	0.000	0.000	0.003	0.002	0.000	0.003
Na	0.226	0.239	0.169	0.205	0.362	0.247	0.287	0.383	0.293	0.008	0.019	0.015	0.014	0.013	0.020	0.016	0.030	0.008
K	0.065	0.059	0.059	0.065	0.065	0.075	0.078	0.092	0.070	0.890	0.867	0.886	0.906	0.902	0.886	0.915	0.869	0.803
Total	15.172	15.190	15.150	15.169	15.285	15.200	15.270	15.364	15.249	7.805	7.814	7.831	7.819	7.838	7.755	7.809	7.822	7.664
X_{Mg}	0.74	0.73	0.74	0.74	0.69	0.73	0.73	0.72	0.72	0.59	0.59	0.57	0.59	0.60	0.60	0.60	0.58	0.58

Rock types: Biotite granodiorite (BG1, BG2); hornblende-biotite granodiorite (HBG); microgranular mafic enclave (ME); dacitic dike (D). X_{Mg} is Mg/(Mg + Fe)

Table 2 Ar–Ar isotope data on two biotite separates from the Saraycık granodiorite

Sample	K (wt%)	^{40}Ar* (nl/g)	^{40}Ar* (%)	^{40}Ar*/^{39}Ar	J value ($\times 10^{-4}$)	Total gas age (Ma)	Plateau age (Ma)
TO1	8.1	16.57 ± 0.16	67.3	9.03 ± 0.08	32.36 ± 0.20	51.9 ± 0.5 (1.2)	–
TO1	8.1	16.64 ± 0.22	44.2	9.01 ± 0.08	32.54 ± 0.35	52.1 ± 0.7 (1.2)	52.8 ± 0.7 (1.2)
479	8.3	16.95 ± 0.13	76.5	9.20 ± 0.07	32.27 ± 0.11	52.8 ± 0.4 (1.2)	–
479	8.3	16.54 ± 0.12	61.6	8.85 ± 0.07	32.93 ± 0.04	51.8 ± 0.4 (1.2)	52.2 ± 0.4 (1.2)

K is estimated from the amount of ^{39}Ar. Errors given are $\pm 1\sigma$. Errors in parentheses comprise age error and uncertainty of standard. An in-house standard, 'Bmus' (Bärhalde muscovite), calibrated against MMHb1, was used; age, K content and ^{40}Ar* content are 326.2 ± 1.1 Ma (1σ), 8.47 wt% and 117.7 nl/g, respectively

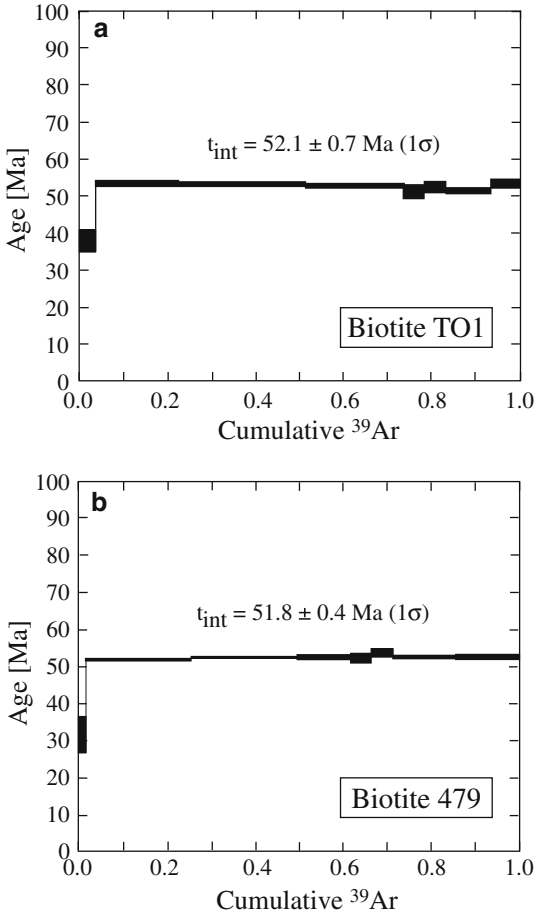

Fig. 4 ^{40}Ar/^{39}Ar incremental spectra of biotites

with Eu/Eu* [= $Eu_{cn}/(Sm_{cn}\cdot Gd_{cn})^{0.5}$] ranging from 0.92 to 1.08 (Fig. 6). $(La/Yb)_{cn}$ ratios are generally high (~43 to 86). While the REE patterns of the dacitic dikes are similar to those of the granodiorites, the aplites are characterized by somewhat lower abundances of REE (Fig. 6, Table 3). The microgranular mafic enclave 547, however, is characterized by higher REE contents, a significant negative Eu anomaly (Eu/Eu* = 0.73) and a lower value of $(La/Yb)_{cn}$ (~32). Primitive mantle-normalized element concentration diagrams of granodiorite and dike rock samples show significant negative anomalies of Nb–Ta, P and Ti in conjunction with a positive anomaly of Pb (Fig. 7). The mafic enclave, however, is characterized by the lack of a positive Pb anomaly and negative anomalies of Sr and Zr–Hf.

Granodiorite and dacite samples from the Saraycık intrusive complex show a distinct 'adakitic flavour', with many chemical signatures being similar to those of high-silica adakites (HSA), such as low contents of garnet-compatible elements (Y, HREE, Sc), high abundances of plagioclase-compatible Sr and Ba (Table 3), high ratios of Sr/Y and La/Yb (Fig. 8), absence of significant Eu anomalies, and concave-upward shapes of chondrite-normalized HREE patterns (Fig. 6). In terms of Mg# vs SiO_2, the rocks plot into the low-Mg#/high-SiO_2 region of the adakite field, as defined by Smithies (2000). Average HSA has 64.8 ± 2.5 (1σ) wt% SiO_2 and Mg# = 47.6 (Martin et al. 2005). Similar to HSA, the Saraycık granodiorites and dacites have low K_2O/Na_2O ratios (except for the two BG1 samples; Table 3). They are, however, slightly more felsic and tend to have slightly higher ASI than most HSA.

Nd–Sr isotopes

Bulk-rock Nd and Sr isotope data are listed in Table 4. Calculated initial Nd and Sr isotopic compositions for the different samples are based on the Ar–Ar age of 52 Ma determined on two biotite separates (see above). All samples have very similar Nd–Sr isotopic characteristics, regardless of rock type and SiO_2 content. Initial ε_{Nd} values range from −0.25 to −1.24 and initial $^{87}Sr/^{86}Sr$ isotope ratios from 0.70491 to 0.70529.

Discussion

Composite nature of the Saraycık pluton

Since the compositional differences among the three types of granodiorite (BG1, BG2, HBG) can hardly be explained by crystal fractionation, it is assumed that these granodiorite types are derived from three distinct magma pulses. Unfortunately, the outcrop situation does not allow to establish an age sequence between the different types of granodiorite. The textures of the dacitic dikes suggest rapid cooling in an already-solidified granodiorite. The aplitic dikes could represent residual felsic melts that were expelled from a compacting

Table 3 Whole-rock analyses of granodioritic, dacitic and aplitic samples from the Saraycık intrusion and of experimentally produced dehydration melts from amphibolites

Sample	TO1	456	478A	479	480*	490	541A	542	544A	545	455	489	547	541D	543	478B	488	548	B4[a]	B5[a]	M4[a]	Rock 1[b]
Rock type	BG1	BG1	BG2	BG2	BG2	BG2	BG2	BG2	BG2	BG2	HBG	HBG	ME	D	D	A	A	A	Exp	Exp	Exp	Exp
SiO_2	69.09	69.67	67.98	70.21	70.34	68.24	68.06	69.87	66.58	69.27	68.27	64.91	50.10	66.93	67.23	77.07	76.45	74.72	70.09	68.10	67.56	69.76
TiO_2	0.25	0.28	0.33	0.25	0.28	0.33	0.36	0.36	0.43	0.34	0.38	0.37	1.46	0.42	0.39	0.07	0.14	0.15	0.54	0.80	0.63	0.85
Al_2O_3	16.56	16.56	16.76	15.73	16.53	16.27	16.25	15.32	17.31	16.12	16.70	18.32	18.41	17.22	16.95	12.77	12.46	13.81	16.10	17.08	17.64	15.59
$Fe_2O_3^{tot}$	1.52	1.62	2.28	1.56	1.74	2.03	2.59	2.42	2.91	2.09	2.24	2.46	9.27	2.73	2.98	0.35	0.67	1.24	2.64	3.31	2.63	3.96
MnO	0.04	0.05	0.03	0.04	0.03	0.04	0.03	0.03	0.03	0.03	0.05	0.04	0.15	0.02	0.05	0.00	0.01	0.02	n.a.	n.a.	n.a.	0.03
MgO	0.49	0.75	0.96	0.65	0.83	0.83	1.39	1.24	1.13	0.90	1.12	1.25	3.96	0.86	1.49	0.00	0.10	0.36	0.69	0.92	0.74	0.71
CaO	1.96	2.37	4.01	1.75	1.10	3.46	3.25	3.18	4.07	3.08	3.89	5.05	5.22	3.87	3.91	0.45	0.82	1.63	2.52	2.97	2.35	3.16
Na_2O	4.83	4.53	4.63	4.69	4.54	4.70	3.85	3.76	4.35	4.48	4.43	5.30	4.81	4.21	4.31	3.72	3.32	3.66	4.64	4.65	5.63	4.50
K_2O	3.77	3.59	2.09	2.77	2.83	2.29	2.40	1.94	1.87	2.38	2.29	1.54	2.91	1.47	1.76	4.97	4.56	3.97	3.05	2.84	3.09	1.81
P_2O_5	0.11	0.12	0.12	0.10	0.12	0.13	0.16	0.14	0.22	0.16	0.16	0.16	1.26	0.18	0.17	0.00	0.04	0.04	n.a.	n.a.	n.a.	n.a.
LOI	0.62	0.30	0.40	0.90	1.40	0.76	1.20	1.30	0.90	0.80	0.53	0.52	2.20	1.20	0.50	0.14	0.44	0.40	n.a.	n.a.	n.a.	n.a.
Total	99.24	99.84	99.59	98.65	99.74	99.08	99.55	99.57	99.81	99.65	100.07	99.92	99.75	99.11	99.74	99.54	99.01	100.01	100.01	100.24	100.01	99.98
Cs	6.8	8.1	1.9	n.a.	6.8	n.a.	10.9	8.8	5.3	3	4.8	n.a.	22.3	13.5	3.5	n.a.	n.a.	2.3	–	–	–	–
Rb	135	127	66	120	110	74	111	86	79	87	77	43	224	71	64	286	137	118	–	–	–	–
Ba	1,202	1,065	700	773	633	789	690	727	703	691	782	733	935	611	671	11	600	637	–	–	–	–
Sr	868	800	847	656	616	770	662	647	812	728	699	898	805	761	698	15	160	328	–	–	–	–
Y	15.4	13.9	6.4	8.2	5.6	6.9	7.9	7.9	6.2	4.6	12.2	10.2	26	7.0	7.5	2.1	6.2	2.6	–	–	–	–
Zr	193	168	116	117	94	117	114	112	139	117	117	108	172	109	103	58	61	62	–	–	–	–
HF	4.0	3.9	3.0	n.a.	2.4	n.a.	3.0	2.9	3.3	3	3.3	n.a.	4.3	2.9	2.8	n.a.	n.a.	2.1	–	–	–	–
Pb	40.6	36.1	n.a.	23.3	n.a.	22.4	n.a.	n.a.	n.a.	n.a.	22.9	20.2	4.7	n.a.	n.a.	50.9	23.1	n.a.	–	–	–	–
Zn	37	42	16	n.a.	32	n.a.	21	20	38	42	39	n.a.	195	16	37	n.a.	n.a.	17	–	–	–	–
Ni	2.3	2.6	3.8	n.a.	3.5	n.a.	8.3	6.6	9.2	6.4	5.4	n.a.	17.4	7.7	8.1	n.a.	n.a.	4.1	–	–	–	–
V	34	34	48	50	28	57	48	48	53	39	58	66	175	53	46	6	24	12	–	–	–	–
Cr	9	12	n.a.	22	n.a.	22	n.a.	n.a.	n.a.	n.a.	23	22	n.a.	n.a.	n.a.	5	7	n.a.	–	–	–	–
Sc	1.0	2.0	2.0	n.a.	3.0	n.a.	3.0	4.0	5.0	4	5	n.a.	10	4	5	n.a.	n.a.	1	–	–	–	–
Nb	26	28	10	17	11	15	14	12	14	12	14	16	36	11	11	10	9	13	–	–	–	–
Ta	1.9	1.6	0.5	n.a.	0.8	n.a.	0.9	0.7	0.8	0.9	1.1	n.a.	1.1	0.7	0.7	n.a.	n.a.	1.2	–	–	–	–
U	2.8	3.2	2.3	n.a.	3.9	n.a.	1.6	2.0	1.4	2.8	1.5	n.a.	3.9	2.3	2.5	n.a.	n.a.	2.6	–	–	–	–
Th	42	35	13	16	13	14	17	16	14	14	15	10	22	11	13	28	32	22	–	–	–	–
La	83.9	75.5	33.8	n.a.	27.9	n.a.	40.5	44.3	45.8	40.5	32.0	n.a.	88.7	40.0	35.3	n.a.	n.a.	22.8	–	–	–	–
Ce	116	106	53	n.a.	42	n.a.	67	70	67	63	52	n.a.	167	60	55	n.a.	n.a.	36	–	–	–	–
Pr	10.6	9.5	5.0	n.a.	4.2	n.a.	6.4	6.8	6.7	5.4	5.3	n.a.	17.3	5.9	5.4	n.a.	n.a.	3	–	–	–	–
Nd	35.9	32.6	18.2	n.a.	15.2	n.a.	23.0	24.2	24.1	18.1	20.7	n.a.	68.3	20.7	19.4	n.a.	n.a.	9.8	–	–	–	–
Sm	4.4	4.0	2.6	n.a.	2.4	n.a.	3.1	3.5	3.5	2.5	3.2	n.a.	10.8	3.0	3.2	n.a.	n.a.	1.2	–	–	–	–
Eu	1.10	0.98	0.74	n.a.	0.60	n.a.	0.92	0.97	0.99	0.69	0.92	n.a.	2.14	0.86	0.87	n.a.	n.a.	0.34	–	–	–	–
Gd	3.06	2.58	1.96	n.a.	1.67	n.a.	2.27	2.32	2.47	1.66	2.35	n.a.	7.36	1.96	2.06	n.a.	n.a.	0.77	–	–	–	–
Tb	0.37	0.30	0.21	n.a.	0.21	n.a.	0.28	0.29	0.26	0.18	0.28	n.a.	1.18	0.24	0.28	n.a.	n.a.	0.09	–	–	–	–
Dy	1.78	1.46	1.07	n.a.	1.03	n.a.	1.46	1.42	1.35	0.91	1.42	n.a.	4.66	1.22	1.38	n.a.	n.a.	0.46	–	–	–	–
Ho	0.30	0.27	0.21	n.a.	0.18	n.a.	0.23	0.25	0.19	0.14	0.26	n.a.	0.84	0.22	0.22	n.a.	n.a.	0.07	–	–	–	–
Er	0.85	0.68	0.46	n.a.	0.46	n.a.	0.64	0.58	0.53	0.36	0.70	n.a.	2.12	0.54	0.63	n.a.	n.a.	0.22	–	–	–	–
Tm	0.14	0.11	0.08	n.a.	0.08	n.a.	0.10	0.11	0.10	0.06	0.11	n.a.	0.30	0.09	0.09	n.a.	n.a.	0.05	–	–	–	–
Yb	1.02	0.85	0.55	n.a.	0.48	n.a.	0.79	0.64	0.63	0.46	0.72	n.a.	1.89	0.65	0.67	n.a.	n.a.	0.34	–	–	–	–
Lu	0.16	0.14	0.09	n.a.	0.07	n.a.	0.12	0.09	0.08	0.07	0.12	n.a.	0.29	0.09	0.10	n.a.	n.a.	0.06	–	–	–	–
Mg#	39.0	47.8	45.5	45.2	48.6	44.8	51.5	50.4	43.5	46.0	49.8	50.2	45.8	38.4	49.8	0	22.8	36.5	34.1	35.5	35.8	26.2
ASI	1.06	1.06	0.98	1.13	1.32	0.99	1.09	1.09	1.04	1.04	0.99	0.94	0.90	1.11	1.05	1.04	1.05	1.04	1.04	1.07	1.05	1.03
(La/Yb)cn	79.3	85.7	59.3	–	56.1	–	49.5	66.8	70.1	84.9	42.9	–	31.6	59.4	50.8	–	–	64.7	–	–	–	–
(Tb/Yb)cn	2.29	2.23	2.41	–	2.76	–	2.24	2.86	2.60	2.47	2.45	–	2.75	2.33	2.64	–	–	1.67	–	–	–	–
Eu/Eu*	0.92	0.93	1.00	–	0.92	–	1.06	1.04	1.03	1.04	1.03	–	0.73	1.08	1.04	–	–	1.08	–	–	–	–

Rock types: biotite granodiorite (BG1 and BG2); hornblende-biotite granodiorite (HBG); microgranular mafic enclave (ME); dacitic dike (D), aplitic dike (A). *Sample 480 is considerably altered (see text). Exp = experimentally produced dehydration melt. [a]Sen and Dunn (1994); [b]Rapp and Watson (1995). Mg# is $100\times MgO/(MgO+FeO_{tot})$ in molar proportions; ASI is the aluminium saturation index [molar $Al_2O_3/(CaO+K_2O+Na_2O)$]. Oxides are given in wt%, trace elements in μg/g. Experimental conditions during dehydration melting were as follows: B4: 950°C/1.5 GPa, B5: 975°C/1.5 GPa, M4: 950°C/1.5 GPa, Rock 1: 1000°C/1.6 GPa

framework of crystal grains at depth. This hypothesis is supported by initial Nd–Sr isotopic ratios that are nearly similar for all types of granodiorite and the dacitic and aplitic dikes (Table 4).

The sparse microgranular mafic enclaves that occur in the eastern part of the pluton suggest limited mingling between small volumes of (monzo)dioritic magma and coexisting granodioritic magma. This view is supported by the presence of two types of plagioclase phenocrysts in the granodiorite and the dacitic dikes. While most plagioclase grains are characterized by normal oscillatory zoning, some are complexly zoned and may originate from magma mixing and mingling (e.g. Baxter and Feely 2002). Since original compositions of the small enclaves (former globules of mafic melt) were probably modified by interaction with the granodioritic host magma (as suggested for other occurrences; e.g. Waight et al. 2000 and references therein), a more thorough discussion of the genesis of the microgranular enclaves is beyond the scope of this paper.

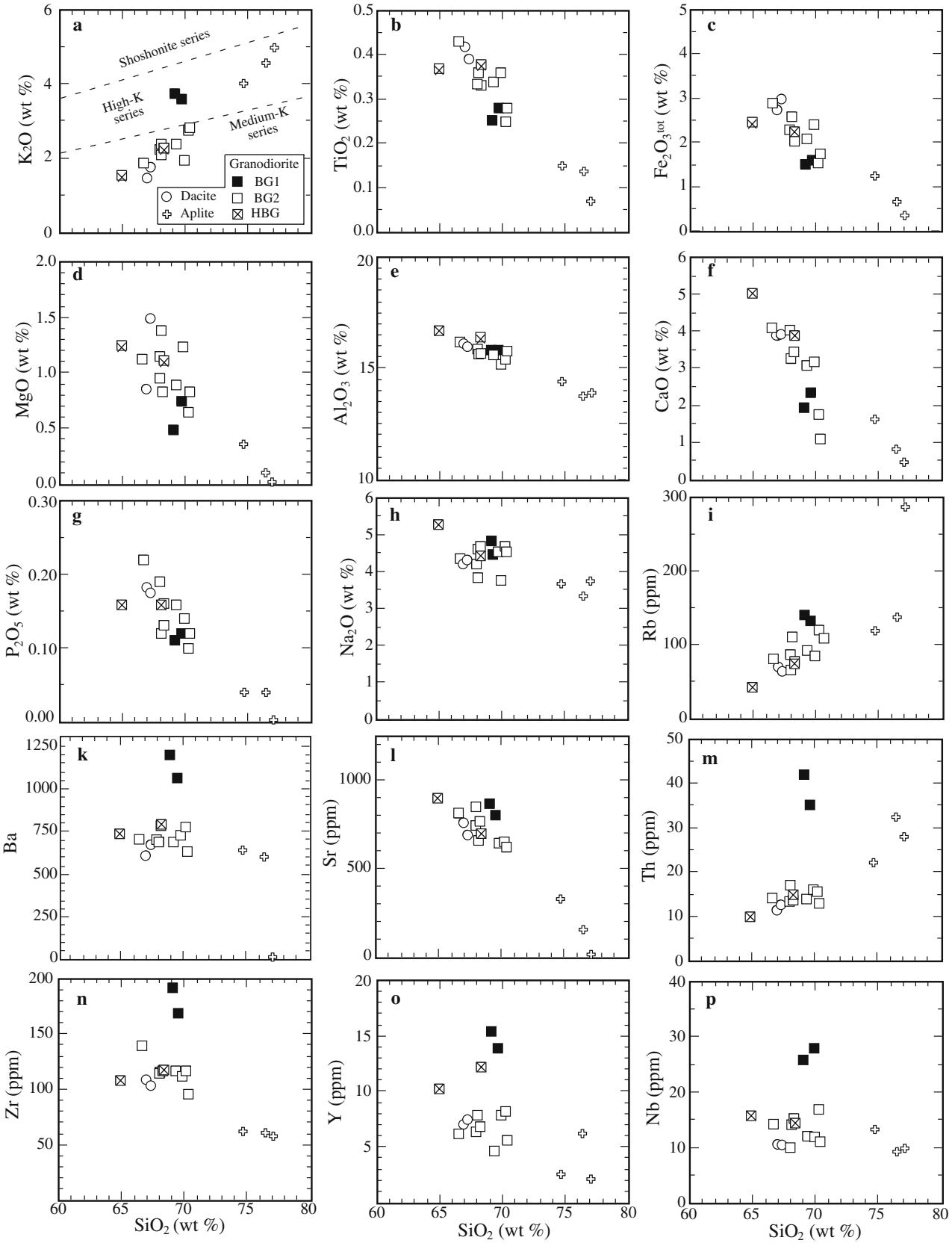

Fig. 5 Harker variation diagrams for samples from the Saraycık intrusion. The diagram of **a** K_2O versus SiO_2 shows field boundaries between medium-K (normal calc-alkaline), high-K and shoshonitic series of Peccerillo and Taylor (1976)

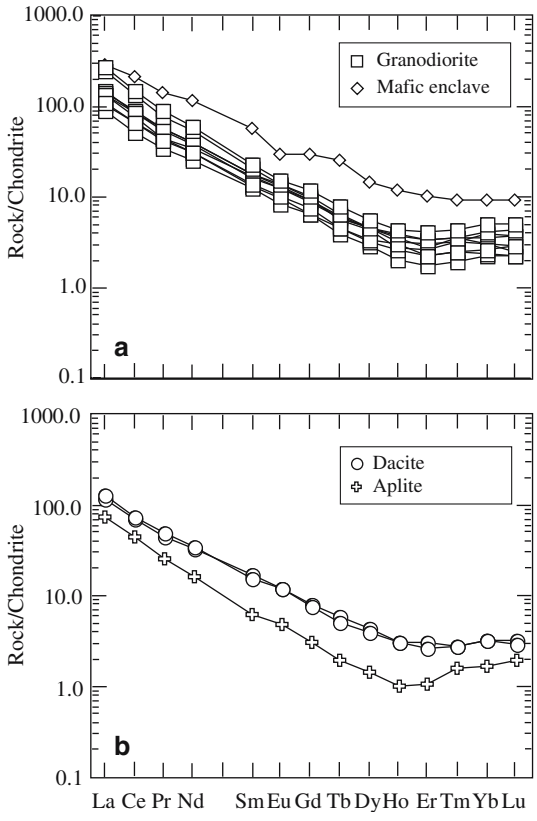

Fig. 6 Chondrite-normalized REE abundance patterns (normalized to values given in Boynton 1984) for selected samples from the Saraycık intrusion. **a** granodiorite and mafic enclave. **b** dacitic and aplitic dikes

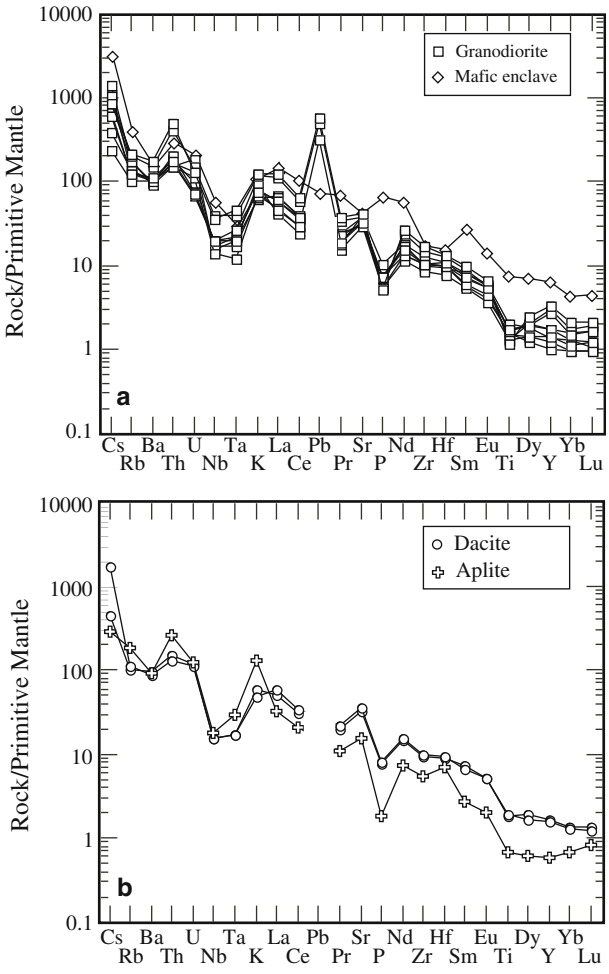

Fig. 7 Primitive mantle-normalized trace element abundance patterns (normalized to values given in Sun and McDonough 1989) for selected samples from the Saraycık intrusion

Temperatures of Saraycık magmas

Temperatures of granitoid magmas may be estimated from apatite and zircon saturation temperatures that can be calculated from chemical compositions of rock samples (Harrison and Watson 1984; Hanchar and Watson 2003, and references therein). For any given melt, saturation temperatures for apatite and zircon components depend on both melt composition and temperature, whereby the solubilities of both components increase with temperature. Apatite and zircon saturation temperatures calculated from bulk-rock chemical analyses will therefore correspond to maximum or minimum temperature limits for the intruding magma depending on whether the melt was saturated or undersaturated in these components.

Zr abundances in granodiorite and dacite samples from the Saraycık intrusion (94–193 μg/g; Table 3) result in zircon saturation temperatures of 730–802°C. Since subhedral zircon grains do not occur in the cores of large plagioclase and hornblende grains, but are abundant in quartz, orthoclase, biotite and the outer parts of plagioclase grains, it is inferred that the crystallization of zircon started relatively late, at temperatures lower than that of the intruding magma. This conclusion is supported by the fact that Zr abundances are not systematically related to SiO_2 contents (Fig. 5m). Therefore, calculated zircon saturation temperatures should be considerably lower than the temperature of the intruding magma. On the other hand, apatite crystallization seems to have started earlier, since apatite grains occur in early crystallized plagioclase and hornblende (as well as in other phases) and bulk-rock P_2O_5 contents decrease with increasing SiO_2 (Fig. 5g). Therefore, the temperatures of the intruding magmas were probably not much higher than the calculated apatite saturation temperatures of 902–958°C.

Magma genesis

Overall geochemical and Nd–Sr isotopic characteristics of the Saraycık adakite-like rocks suggest an origin by partial melting of a mafic source at pressures high enough to stabilize a residual mineral assemblage rich in garnet ± amphibole and poor in plagioclase. This implies a minimum pressure of ~1 GPa (e.g. Wyllie and Wolf 1993; López and Castro 2001). The formation of

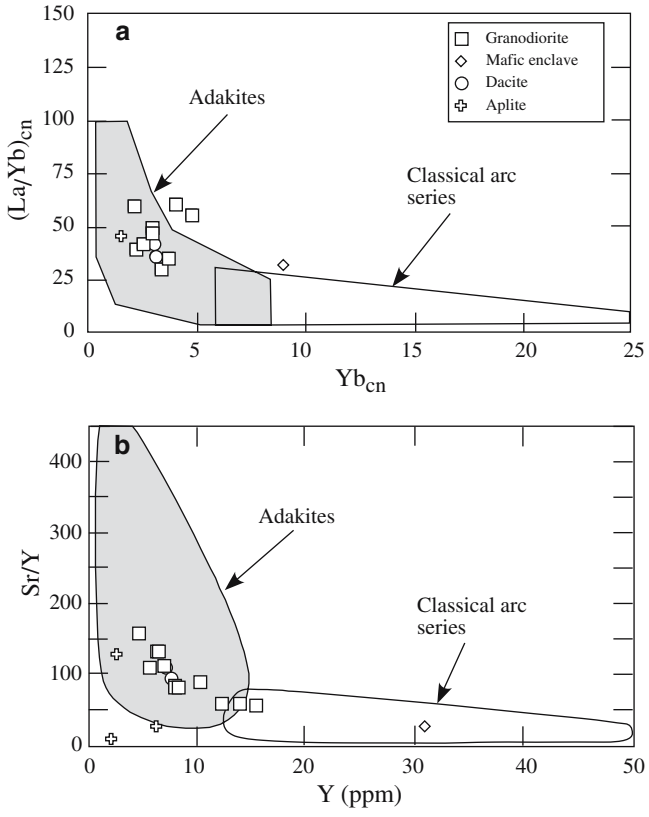

Fig. 8 **a** Chondrite-normalized La/Yb ratios versus chondrite-normalized Yb abundances in rocks from the Saraycık intrusion. **b** Sr/Y versus Y in the same samples

the intrusive complex within a post-collisional setting excludes the possibility of slab melting in conjunction with melt-peridotite interaction. Instead, derivation of magmas from the mafic lower crust seems probable. The necessary heat for partial melting of the lower crust can be provided by repetitive underplating with basaltic magmas (e.g. Petford and Gallagher 2001; Annen and Sparks 2002). Several experimental studies have shown that lower continental crustal temperatures need not be unrealistically high to produce granitoid liquids during garnet-amphibolite dehydration melting. In the garnet-absent field, at pressures <1 GPa, amphibolites begin to melt at relatively high temperatures of 800–900°C, but at ~1 GPa, the solidus backbends and at higher pressure, dehydration melting begins at temperatures as low as ~750°C (e.g. Wyllie and Wolf 1993; Wolf and Wyllie 1991, 1994; López and Castro 2001).

Compositions of melts produced by partial melting of mafic lower crust depend on (1) source composition, (2) water content (dehydration melting vs wet melting) and (3) *P–T* conditions and degree of melting. Most experiments have been carried out on MORB-like compositions with low K_2O contents. Partial melts produced from these compositions at pressures between 1 and 2 GPa and temperatures $\leq$ 1,000°C are generally characterized by low K_2O (<1.8 wt%, mostly <1.2 wt%) and K_2O/Na_2O ratios (<0.34, mostly <0.25), regardless of the amount of H_2O being present in the system (Rapp et al. 1991; Winther and Newton 1991; Rapp and Watson 1995; Wolf and Wyllie 1994; Winther 1996; Prouteau et al. 2001; López and Castro 2001). These values are significantly lower than those shown by the Saraycık rocks (Table 3). Only in systems with elevated K_2O content (~0.8 wt%), partial melts are characterized by higher K_2O contents and ratios of K_2O/Na_2O (up to 1.3, mostly <0.8) (Rapp et al. 1991; Sen and Dunn 1994; Rapp 1995; Rapp and Watson 1995).

Table 4 Rb–Sr and Sm–Nd isotopic data for the Saraycık pluton

Sample	Rb (ppm)	Sr (ppm)	Sm (ppm)	Nd (ppm)	$^{87}Rb/^{86}Sr$	$^{87}Sr/^{86}Sr$	$^{87}Sr/^{86}Sr(I)$	$^{147}Sm/^{144}Nd$	$^{143}Nd/^{144}Nd$	$^{143}Nd/^{144}Nd(I)$	$\varepsilon_{Nd}(I)$	T_{DM} [Ga]
Granodiorite (type)												
TO1 (BG1)	143	893	4.4	35.9	0.463	0.705546(08)	0.70520	0.0744	0.512553(10)	0.512528	−0.85	0.63
456 (BG1)	144	872	4.0	32.6	0.478	0.705529(09)	0.70518	0.0745	0.512557(07)	0.512532	−0.77	0.63
478A (BG2)	66	847	2.6	18.2	0.225	0.705075(08)	0.70491	0.0867	0.512572(09)	0.512542	−0.56	0.67
480 (BG2)	110	616	2.4	15.2	0.517	0.705646(10)	0.70526	0.0959	0.512540(08)	0.512507	−1.24	0.76
541A (BG2)	111	662	3.1	23.0	0.485	0.705443(07)	0.70509	0.0818	0.512586(05)	0.512558	−0.25	0.63
542 (BG2)	86	647	3.5	24.2	0.384	0.705451(09)	0.70517	0.0878	0.512574(07)	0.512544	−0.53	0.67
544A (BG2)	79	812	3.5	24.1	0.281	0.705301(09)	0.70510	0.0882	0.512575(08)	0.512545	−0.51	0.67
545 (BG2)	87	728	2.5	18.1	0.346	0.705177(10)	0.70492	0.0839	0.512570(10)	0.512541	−0.58	0.66
455 (HBG)	87	751	3.2	20.7	0.335	0.705323(10)	0.70508	0.0939	0.512577(08)	0.512545	−0.51	0.70
Dacitic dikes												
541D	71	761	3.0	20.7	0.270	0.705493(09)	0.70529	0.0880	0.512543 ± 10	0.512513	−1.13	0.71
543	64	698	3.2	19.4	0.265	0.705261(07)	0.70507	0.1002	0.512559 ± 10	0.512525	−0.90	0.76
Aplitic dike												
548	118	328	1.2	9.8	1.041	0.705741(10)	0.70497	0.0744	0.512571 ± 10	0.512546	−0.50	0.61

Uncertainties for the $^{87}Sr/^{86}Sr$ and $^{143}Nd/^{144}Nd$ ratios are $2\sigma_m$ errors in the last two digits (in parantheses). $\varepsilon_{Nd}(I)$ values (at 52 Ma) are calculated relative to CHUR with present day values of $^{143}Nd/^{144}Nd = 0.512638$ and $^{147}Sm/^{144}Nd = 0.1967$ (Jacobsen and Wasserburg 1980). Nd model ages (T_{DM}) are calculated with a depleted-mantle reservoir and present-day values of $^{144}Nd/^{143}Nd = 0.513151$ and $^{147}Sm/^{144}Nd = 0.219$ (e.g. Liew and Hofmann 1988)

Melt fractions produced by dehydration melting of amphibolite at 1.0–1.5 GPa and 900°C are small (≤ 5%) and compositions are essentially granitic. Only at higher temperatures of ~950–975°C, melt fractions increase considerably (up to 20%) and the melts become granodioritic (e.g. Sen and Dunn 1994; López and Castro 2001). Compositions of some experimentally produced dehydration melts that are roughly similar to those of the Saraycık granodiorites and dacites are listed in Table 3. These granodioritic melts formed in basaltic systems with ~0.8 wt% K_2O at temperatures of 950–1,000°C and pressures of 1.5–1.6 GPa (Sen and Dunn 1994; Rapp and Watson 1995). Compared to the Saraycık granodiorites and dacites, experimentally produced melt compositions consistently show lower Mg# values (Table 3). A close inspection of melt compositions generated by both dehydration and wet melting (references given above) reveals that at given *P* and *T*, Mg# values of partial melts are primarily controlled by Mg# of the source and by the degree of partial melting, whereby the latter increases with the amount of water present in the system. If the Saraycık magmas were produced by dehydration melting at ~1.5 GPa and 950–1,000°C, the source must have been characterized by elevated K_2O contents and high Mg# (near to 70). ASI values of dehydration melts produced at 1–2 GPa range from 0.90 to 1.18, depending on source composition and degree of partial melting. This range of ASI values comprises the values of Saraycık magmas (Table 3).

Melt fractions and compositions produced by wet melting of a basaltic source at given *P* and *T* will strongly depend on the amount of H_2O available in the system. Details of these relationships are unfortunately not known, since relevant experimental data are limited (Winther and Newton 1991; Winther 1996; Prouteau et al. 2001). Granodioritic melts could be produced at temperatures lower than those needed during dehydration melting. However, large amounts of H_2O are unlikely to be present in the lower crust.

In conclusion, we suggest that the adakite-like Saraycık magmas were generated by dehydration melting of mafic lower crust at pressures of 1–2 GPa, leaving behind a residue rich in garnet ± amphibole. Compared to MORB, the source must have been characterized by higher K_2O contents and Mg#.

Conclusions and geodynamic implications

Eocene I-type granitoid plutons are widespread in the Eastern Pontides (e.g. Gedik et al. 1992; Yılmaz and Boztuğ 1996; Okay and Şahintürk 1997; Boztuğ et al. 2004). For most of these plutons, detailed data on their ages and compositional characteristics are unfortunately not yet available impeding regional correlations and a more general picture of post-collisional magmatism in the eastern Pontides. However, this study on the Saraycık intrusion yields at least some constraints on both the age of tectonic events and the thermal state of the lower crust shortly after the collision between the Pontides in the North and the Anatolide-Tauride passive margin in the South.

The Saraycık pluton pierced the Pulur thrust separating the Asutka from the Hamurkesen thrust sheets. Therefore, the intrusion age of 52 Ma (Ypresian) estimated from concordant Ar–Ar ages on two biotite separates provides a minimum age for the formation of the Paleogene north-vergent fold-and-thrust belt of the Eastern Pontides. Local shear zones observed within the pluton may either represent late-stage convergent or extensional movements.

Coherent geochemical signatures and a narrow range of Nd–Sr isotope compositions of both the granodiorite and the dacitic and aplitic dike rocks suggest a comagmatic nature of the different magma batches and preclude significant assimilation of crustal materials during magma ascent and intrusion at upper crustal levels (~5–8 km below surface). An origin by pure remagmatization (dehydration melting) of older mafic lower crust is regarded as the most viable model for generating the adakite-like chemical signatures. The lowermost crust must have been relatively hot (≥950°C) implying extensive heating by mantle-derived mafic magmas (Petford and Gallagher 2001; Annen and Sparks 2002).

Acknowledgements This paper benefited from constructive reviews by two anonymous referees, discussions with Aral I. Okay, Cüneyt Şen and Cemal Göncüoğlu, and from logistic support by Burhan Sadıklar. Special thanks are due to Ilona Fin and Oliver Wienand for preparing thin sections, Hans-Peter Meyer and Thomas Ludwig for their never-ending assistance during XRF and EPMA work, and Ömer Gündüz (†), Osman Nuri Albayrak and Canpulat Hatko for their help during sample preparation. Mutlu Sarıkaya and Özgür Parlak are thanked for their companionship during field work. We are also indebted to the people living in the Saraycık area for their great hospitality and friendliness.

References

Akın H (1979) Geologie, Magmatismus und Lagerstättenbildung im ostpontischen Gebirge/Türkei aus der Sicht der Plattentektonik. Geol Rundschau 68:253–283

Akıncı ÖT (1984) The Eastern Pontide volcano-sedimentary belt and associated massive sulfide deposits. In: Dixon JE, Robertson AHF (eds) The geological evolution of the eastern Mediterranean. Geol Soc Lond Spec Publ, vol 17, pp 415–428

Altherr R, Siebel W (2002) I-type plutonism in a continental back-arc setting: Miocene granitoids and monzonites from the central Aegean Sea, Greece. Contrib Mineral Petrol 143:397–415

Altherr R, Holl A, Hegner E, Langer C, Kreuzer H (2000) High-potassium, calc-alkaline I-type plutonism in the European Variscides: northern Vosges (France) and northern Schwarzwald (Germany). Lithos 50:51–73

Anderson JL, Smith DR (1995) The effect of temperature and oxygen fugacity on Al-in-hornblende barometry. Am Mineral 80:549–559

Annen C, Sparks RSJ (2002) Effects of repetitive emplacement of basaltic intrusions on thermal evolution and melt generation in the crust. Earth Planet Sci Lett 203:937–955

Arslan M, Tüysüz N, Korkmaz S, Kurt H (1997) Geochemistry and petrogenesis of the Eastern Pontide volcanic rocks, Northeast Turkey. Chem Erde 57:157–187

Atherton MP, Petford N (1993) Generation of sodium-rich magmas from newly underplated basaltic crust. Nature 362:144–146

Baxter S, Feely M (2002) Magma mixing and mingling textures in granitoids: examples from the Galway granite, Connemara, Ireland. Mineral Petrol 76:63–74

Boynton WV (1984) Cosmochemistry of the rare earth elements: meteorite studies. In: Henderson P (ed) Rare earth element geochemistry. Elsevier, Amsterdam, pp 63–114

Boztuğ D, Jonckheere R, Wagner GA, Yegingil Z (2004) Slow Senonian and fast Palaeocene-Early Eocene uplift of the granitoids in the Central Eastern Pontides, Turkey: apatite fission-track results. Tectonophysics 382:213–228

Chung S-L, Liu D, Ji J, Chu M-F, Lee H-Y, Wen D-J, Lo C-H, Lee T-Y, Qian Q, Zhang Q (2003) Adakites from continental collision zones: melting of thickened lower crust beneath southern Tibet. Geology 31:1021–1024

Condie KC (2005) TTGs and adakites: are they both slab melts? Lithos 80:33–44

Defant MJ, Drummond MS (1990) Derivation of some modern arc magmas by partial melting of young subducted lithosphere. Nature 347:662–665

Defant MJ, Drummond MS (1993) Mount St. Helens: potential example of the partial melting of the subucted lithosphere in a volcanic arc. Geology 21:547–550

Drummond MS, Defant MJ (1990) A model for trondhjemite-tonalite-dacite genesis and crustal growth via slab melting: archean to modern comparisons. J Geophys Res 95:21503–21521

Gao S, Rudnick RL, Yuan H-L, Liu X-M, Liu Y-S, Xu W-L, Ling W-L, Ayers J, Wang X-C, Wang Q-H (2004) Recycling lower continental crust in the North China craton. Nature 432:892–897

Garrison JM, Davidson JP (2003) Dubious case for slab melting in the Northern volcanic zone of the Andes. Geology 31:565–568

Gedik A, Ercan T, Korkmaz S, Karatas S (1992) Rize-Fındıklı-Çamlıhemsin arasında (Doğu Karadeniz) yer alan magmatik kayaçların petrolojisi ve Doğu Pontidlerdeki bölgesel yayılımları. Türkiye Jeoloji Bülteni 35:15–38

Gedikoğlu A, Pelin S, Özsayar T (1979) The main lines of geotectonic development of the East Pontides in the Mesozoic era. In: Proceedings of the 1st Geol Congr Middle East (GEOCOME), pp 555–580

Grove M, Harrison TM (1996) ^{40}Ar diffusion in Fe-rich biotite. Am Mineral 81:940–951

Hanchar JM, Watson EB (2003) Zircon saturation thermometry. In: Hanchar JM, Hoskin PWO (eds) Zircon. Rev in Mineralogy and Geochemistry, vol 53. Mineralogical Society of America, Geochemical Society of America, pp 89–112

Harrison TM, Watson EB (1984) The behavior of apatite during crustal anatexis: equilibrium and kinetic considerations. Geochim Cosmochim Acta 48:1467–1477

Harrison TM, Duncan I, McDougall I (1985) Diffusion of ^{40}Ar in biotite: temperature, pressure and compositional effects. Geochim Cosmochim Acta 49:2461–2468

Hradetzky H, Lippolt HJ (1998) K–Ar dating of amphibole bearing rocks in the Schwarzwald, SW Germany. II. Multiple sample ^{40}Ar/^{39}Ar systematics on three metabasites. Neues Jahrb Mineral Mh 1998:119–142

Jacobsen SB, Wasserburg GJ (1980) Sm–Nd isotopic evolution of chondrites. Earth Planet Sci Lett 50:139–155

Jaeger JC (1957) The temperature in the neighborhood of a cooling intrusive sheet. Am J Sci 255:306–318

Johannes W, Holtz F (1996) Petrogenesis and experimental petrology of granitic rocks. Springer, Berlin Heidelberg New York, p 33

Kay SM, Ramos VA, Marquez M (1993) Evidence in Cerro Pampa volcanic rocks for slab melting prior to ridge-trench collision in Southern South America. J Geol 101:703–714

Liew TC, Hofmann AW (1988) Precambrian crustal components, plutonic associations, plate environment of the Hercynian Fold Belt of central Europe: indications from a Nd and Sr isotopic study. Contrib Mineral Petrol 98:129–138

López S, Castro A (2001) Determination of the fluid-absent solidus and supersolidus phase relationships of MORB-derived amphibolites in the range 4–14 kbar. Am Mineral 86:1396–1403

Martin H, Smithies RH, Rapp R, Moyen J-F, Champion D (2005) An overview of adakite, tonalite-trondhjemite-granodiorite (TTG), and sanukitoid: relationships and some implications for crustal evolution. Lithos 79:1–24

Okay AI (1986) High-pressure/low-temperature metamorphic rocks of Turkey. Geol Soc Am Memoir 164:333–347

Okay AI (2000) Was the Late Triassic orogeny in Turkey caused by the collision of an oceanic plateau? In: Bozkurt E, Winchester JA, Piper JDA (eds) Tectonic and magmatism in Turkey and surrounding area. Geol Soc London Spec Publ, vol 173, pp 25–41

Okay AI, Kelley SP (1994) Tectonic setting, petrology and geochronology of jadeite + glaucophane and chloritoid + glaucophane schists from northwest Turkey. J Metamorphic Geol 12:455–466

Okay AI, Monié P (1997) Early Mesozoic subduction in the Eastern Mediterranean: evidence from Triassic eclogite in the northwest Turkey. Geology 25:595–598

Okay AI, Şahintürk Ö (1997) Geology of the Eastern Pontides. In: Robinson AG (ed) Regional and petroleum geology of the Black Sea and surrounding region. AAPG Memoir, vol 68, pp 291–311

Okay AI, Satır M, Maluski H, Siyako M, Monié P, Metzger R, Akyüz S (1996) Palaeo- and Neo-Tethyan events in northwest Turkey. In: Yin E, Harrison M (eds) Tectonics of Asia. Cambridge University Press, Cambridge, pp 420–441

Okay AI, Şahintürk Ö, Yakar H (1997) Stratigraphy and tectonics of the Pulur (Bayburt) region in the eastern Pontides. Mineral Res Exp Bull 119:1–24

Okay AI, Monod O, Monié P (2002) Triassic blueschists and eclogites from northwest Turkey: vestiges of the Paleo-Tethyan subduction. Lithos 64:155–178

Pattison DRM, Spear FS, Debuhr CL, Cheney JT, Guidotti CV (2002) Thermodynamic modelling of the reaction muscovite + cordierite–> Al_2SiO_5 + biotite + quartz + H_2O: constraints from natural assemblages and implications for the metapelitic petrogenetic grid. J Metam Geol 20:99–118

Peccerillo A, Taylor SR (1976) Geochemistry of Eocene calc-alkaline volcanic rocks from the Kastamonu area, northern Turkey. Contrib Mineral Petrol 58:63–81

Petford N, Gallagher K (2001) Partial melting of mafic (amphibolitic) lower crust by periodic influx of basaltic magma. Earth Planet Sci Lett 193:483–499

Pouchou JL, Pichoir F (1984) A new model for quantitative analyses. I. Application to the analysis of homogeneous samples. La Recherche Aérospatiale 3:13–38

Pouchou JL, Pichoir F (1985) "PAP" ($\phi{\cdot}\rho{\cdot}$Z) correction procedure for improved quantitative microanalysis. In: Armstrong JT (ed) Microbeam analysis. San Francisco Press, pp 104–106

Prouteau G, Scaillet B (2003) Experimental constraints on the origin of the 1991 Pinatubo dacite. J Petrol 44:2203–2241

Prouteau G, Scaillet B, Pichavant M, Maury R (2001) Evidence for mantle metasomatism by hydrous silicic melts derived from subducted oceanic crust. Nature 410:197–200

Rapp RP (1995) Amphibole-out phase boundary in partially melted metabasalt, its control over liquid fraction and composition, and source permeability. J Geophys Res 100:15601–15610

Rapp RP, Watson EB (1995) Dehydration melting of metabasalt at 8–32 kbar: implications for continental growth and crust-mantle recycling. J Petrol 36:891–931

Rapp RP, Watson EB, Miller CF (1991) Partial melting of amphibolite/eclogite and the origin of Archean trondhjemites and tonalites. Precambrian Res 51:1–25

Rapp RP, Shimizu N, Norman MD, Applegate GS (1999) Reaction between slab-derived melts and peridotite in the mantle wedge: experimental constraints at 3.8 GPa. Chem Geol 160:335–356

Rapp RP, Shimizu N, Norman MD (2003) Growth of early continental crust by partial melting of eclogite. Nature 425:605–609

Rapp RP, Laporte D, Martin H (2005) Interactions between the subducting slab and the mantle wedge during adakite petrogenesis: experimental constraints at 1.5–4.0 GPa. Geophys Res. Abstracts 7, 08116

Robinson AG, Banks CJ, Rutherford MM, Hirst JPP (1995) Stratigraphic and structural development of the Eastern Pontides, Turkey. J Geol Soc Lond 152:861–872

Schubert W, Lippolt HJ, Schwarz W (2001) Early to Middle Carboniferous hornblende $^{40}Ar/^{39}Ar$ ages of amphibolites and gabbros from the Berstraesser Odenwald. Mineral Petrol 72:113–132

Sen C, Dunn T (1994) Dehydration melting of a basaltic composition amphibolite at 1.5 and 2.0 GPa: implications for the origin of adakites. Contrib Mineral Petrol 117:394–409

Şen C, Arslan M, Van A (1998) Geochemical and petrological characteristics of the Eastern Pontide Eocene (?) alkaline volcanic province, NE Turkey. Turkish J Earth Sci 7:231–239

Şengör AMC, Yılmaz Y (1981) Tethyan evolution of Turkey: a plate tectonic approach. Tectonophysics 75:181–241

Smith DR, Leeman WP (1987) Petrogenesis of Mount St. Helens dacitic magmas. J Geophys Res 92:10313–10334

Smithies RH (2000) The Archaean tonalite-trondhjemite-granodiorite (TTG) series is not an analogue of Cenozoic adakite. Earth Planet Sci Lett 182:115–125

Steiger RH, Jäger E (1977) Subcommission on geochronology: convention on the use of decay constants in geo- and cosmochronology. Earth Planet Sci Lett 36:359–362

Stern CR, Kilian R (1996) Role of the subducted slab, mantle wedge and continental crust in the generation of adakites from the Andean Austral Volcanic Zone. Contrib Mineral Petrol 123:263–281

Stevenson JA, Daczko NR, Clarke GL, Pearson N, Kleipeis KA (2005) Direct observation of adakite melts generated in the lower continental crust, Fiordland, New Zealand. Terra Nova 17:73–79

Sun S-S, McDonough WF (1989) Chemical and isotopic systematics of oceanic basalts: implications for mantle composition and processes. In: Saunders AD, Norry MJ (eds) Magmatism in the Ocean Basins. Geol Soc Lond Spec Publ, vol 42, pp 313–345

Tokel S (1977) Doğu Karadeniz Bölgesinde Eoson yaslı kalkalkalen andezitler ve jeotektonizma. Türkiye Jeoloji Kurumu Bülteni 20:49–54

Topuz G, Altherr R, Satır M, Schwarz WH (2004a) Low-grade metamorphic rocks from the Pulur complex, NE Turkey: implications for the pre-Liassic evolution of the Eastern Pontides. Int J Earth Sci 93:72–91

Topuz G, Altherr R, Kalt A, Satır M, Werner O, Schwarz WH (2004b) Aluminous granulites from the Pulur complex, NE Turkey: a case of partial melting, efficient melt extraction and crystallisation. Lithos 72:183–207

Villa IM (1998) Isotopic closure. Terra Nova 10:42–47

Waight TE, Dean AA, Maas R, Nicholls IA (2000) Sr and Nd isotopic investigations towards the origin of feldspar megacrysts in microgranular enclaves in two I-type plutons of the Lachlan Fold Belt, southeast Australia. Aust J Earth Sci 47:1105–1112

Wang Q, McDermott F, Xu J-F, Bellon H, Zhu Y-T (2005) Cenozoic K-rich adakitic volcanic rocks in the Hohxil area, northern Tibet: lower-crustal melting in an intracontinental setting. Geology 33:465–468

Wareham CD, Millar IL, Vaughan APM (1997) The generation of sodic granitic magmas, western Palmer Land, Antarctic Peninsula. Contrib Mineral Petrol 128:81–96

Winther KT (1996) An experimentally based model for the origin of tonalitic and trondhjemitic melts. Chem Geol 127:43–59

Winther KT, Newton RC (1991) Experimental melting of hydrous low-K tholeiite: evidence on the origin of Archaean cratons. Bull geol Soc Denmark 39:213–228

Wolf MB, Wyllie PJ (1991) Dehydration-melting of solid amphibolite at 10 kbar: textural development, liquid interconnectivity and applications to the segregation of magmas. Mineral Petrol 44:151–179

Wolf MB, Wyllie PJ (1994) Dehydration-melting of amphibolite at 10 kbar: the effects of temperature and time. Contrib Mineral Petrol 115:369–383

Wyllie PJ, Wolf MB (1993) Amphibolite dehydration-melting: sorting out the solidus. In: Prichard HM, Alabaster T, Harris NBW, Neary CR (eds) Magmatic processes and plate tectonics. Geol Soc London Spec Publ, vol 76, pp 405–416

Xu JF, Shinjio R, Defant MJ, Wang Q, Rapp RP (2002) Origin of Mesozoic adakitic intrusive rocks in the Ningzhen area of east China: partial melting of delaminated lower continental crust? Geology 32:1111–1114

Yılmaz S, BoztuğD (1996) Space and time relations of three plutonic phases in the Eastern Pontides, Turkey. Intern Geol Rev 38:935–956

Yılmaz Y, Tüysüz O, Yiğitbas E, Genç SC, Şengör AMC (1997) Geology and tectonic evolution of the Pontides. In: Robinson AG (ed) Regional and petroleum geology of the Black Sea and surrounding region. AAPG Memoir, vol 68, pp 183–226

Yumul GP, Dimalanta CB, Bellon H, Faustino DV, De Jesus JV, Tamayo RA, Jumawan FT (2000) Adakitic lavas in the Central Luzon back-arc region, Philippines: lower crustal partial melting products? The Island Arc 9:499–512